PNAS
www.pnas.org

Supplementary Information for

Switch-like activation of Bruton's tyrosine kinase by membrane-mediated dimerization

Jean K. Chung,[a,g,1] Laura M. Nocka,[a,1] Aubrianna Decker, [b] Qi Wang,[b,h] Theresa A. Kadlecek,[d] Arthur Weiss,[d,e,f] John Kuriyan,[a,b,c,2] Jay T. Groves[a,2]

[a]Department of Chemistry, [b]Department of Molecular and Cell Biology, [c] Howard Hughes Medical Institute, University of California, Berkeley, Berkeley, CA 94720, USA
[d]Department of Microbiology and Immunology
[e]Division of Rheumatology, Department of Medicine
[f]The Howard Hughes Medical Institute
University of California, San Francisco, San Francisco, CA 94143, USA
[g]Present address: Department of Chemistry, Colorado State University, Fort Collins, CO 80523, USA
[h]Present address: D. E. Shaw Research, New York, NY 10036, USA
[1]J.K.C. and L.M.N. contributed equally to this work.
[2]To whom correspondence should be addressed. Email: kuriyan@berkeley.edu (J.K.) or jtgroves@lbl.gov (J.T.G.)

This PDF file includes:

www.pnas.org/cgi/doi/10.1073/pnas.1819309116

Contents

1. TIRF calibration

For the kinetic adsorption measurements, the surface density was measured by bulk TIRF, which was calibrated against FCS density measurements. The dimer interface mutant was used for the calibration to avoid complications arising from dimerization. For the experimental range of 0 – 1000 molecules per μm^2, the TIRF intensity was linear with the surface density.

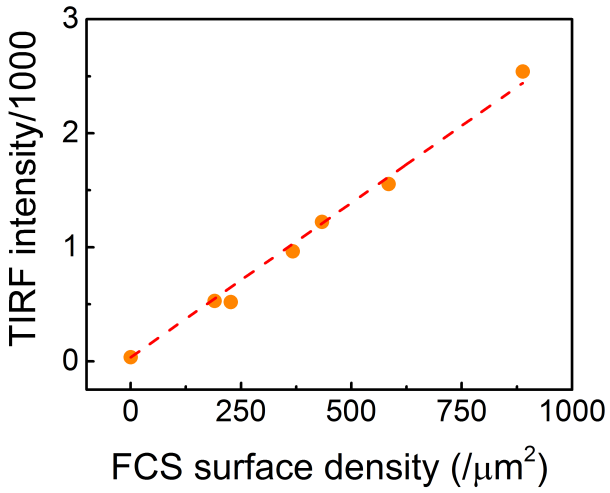

Figure S1. TIRF calibration TIRF intensity was calibrated against surface density measured by FCS with the dimer interface mutant.

2. The canonical site mutant

Mutation of the canonical site (N24D/R28C) in the Btk PH-TH module results in no observable membrane binding. From this observation we conclude PIP_3-binding at the first kinetic step in membrane binding is through the canonical site. This may also suggest that the binding of PIP3 to the peripheral binding site is dependent on the canonical site binding, possibly through an allosteric change—in other words, the binding affinity of the peripheral site for PIP_3 is nonexistent unless the canonical site is already occupied. Molecular dynamics simulations reported previously indicate that PIP_3 binding to the peripheral site results in opening of the otherwise closed Saraste-dimer interface (1). Furthermore, it is important to consider that these rate constants are complicated by a switch from 3D to 2D binding once Btk is recruited through the canonical site, and it is possible that 3D recruitment through the peripheral site exhibits different kinetics than those restricted to 2D (as is the case once Btk is bound to the membrane through the canonical site).

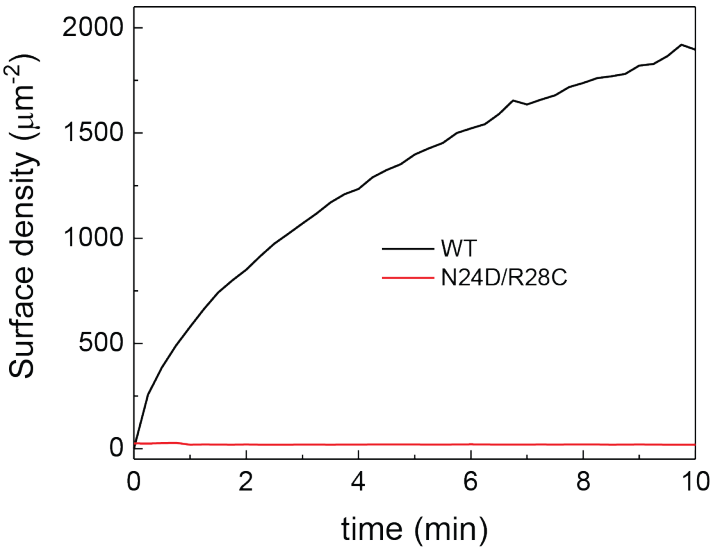

Figure S2. Membrane adsorption of the canonical site mutant, N24D/R28C. When PIP_3 binding at the canonical site is disrupted by the N24D/R28C mutation, there is negligible membrane recruitment, suggesting that the first kinetic step seen in the wild type is due to PIP_3 binding at the canonical site. [PIP_3] = 4%, [WT] = 10 nM, [N24D/R28C] = 20 nM.

3. Estimating kinetic rate constants from TIRF adsorption

We have three Btk PH domain constructs: the wild type, dimer interface mutant, and the peripheral site mutant. Each construct has a distinct adsorption kinetic profile (Figure 4A). We will use this adsorption kinetics data to construct a model for Btk PH domain binding to the PIP_3 membrane followed by dimerization.

As described in the main text, the simplest model for the wild type, in three sequential steps, is:

1. PIP_3 binding at the canonical site
2. PIP_3 binding at the peripheral site, after adsorption
3. Dimerization

First two steps are simply:

(1) Btk + PIP_3 ↔ Btk:PIP_3 (k_1/k_{-1} fwd/rev rate constants; canonical site binding)

(2) Btk:PIP_3 + PIP_3 ↔ Btk:$(PIP_3)_2$ (k_2/k_{-2} fwd/rev rate constants; peripheral site binding)

Two possibilities for the third step, dimerization, were considered. In the first case, each PH domain will be required to bind to two PIP_3 lipids in order to dimerize.

(3a) 2Btk:$(PIP_3)_2$ ↔ Btk_2:$(PIP_3)_4$ (k_{3a}/k_{-3a} fwd/rev rate constants)

In the other case, only one PH domain is required to be bound to two PIP_3:

(3b) Btk:$(PIP_3)_2$ + Btk:PIP_3 ↔ Btk_2:$(PIP_3)_3$ (k_{3b}/k_{-3b} fwd/rev rate constants)

Model A will follow the steps (1) → (2) → (3a), and **Model B** will follow (1) → (2) → (3b).

We will use the simplified notation

B = Btk

P = PIP_3

Then, the mass action rate laws are:

Model A:

$$d[B]/dt = -k_1[B][P] + k_{-1}[BP]$$
$$d[P]/dt = -k_1[B][P] + k_{-1}[BP] - k_2[BP] + k_{-2}[BP_2]$$
$$d[BP]/dt = k_1[B][P] - k_{-1}[BP] - k_2[P][BP] + k_{-2}[BP_2]$$
$$d[BP_2]/dt = k_2[BP][P] - k_{-2}BP_2 - 2k_{3a}[BP_2]^2 + 2k_{-3a}[B_2P_4]$$
$$d[B_2P_4]/dt = k_{3a}[BP_2]^2 - k_{-3a}[B_2P_4]$$

Model B:

$$d[B]/dt = -k_1[B][P] + k_{-1}[BP]$$
$$d[P]/dt = -k_1[B][P] + k_{-1}[BP] - k_2[BP] + k_{-2}[BP_2]$$
$$d[BP]/dt = k_1[B][P] - k_{-1}[BP] - k_2[P][BP] + k_{-2}[BP_2] - k_{3b}[BP][BP_2] + k_{-3b}[B_2P_3]$$
$$d[BP_2]/dt = k_2[BP][P] - k_{-2}BP_2 - k_{3b}[BP][BP_2] + k_{-3b}[B_2P_3]$$
$$d[B_2P_3]/dt = k_{3b}[BP][BP_2] - k_{-3b}[B_2P_3]$$

The kinetic constants will be estimated by fitting the TIRF data with these two models. This was accomplished by sequentially fitting each mutant construct, as illustrated in Figure 4A.

For the peripheral site mutant the reaction cannot proceed past the first binding step (through the canonical site), meaning $k_2 = k_3 = 0$. The coupled kinetic equations are then reduced to

$$d[B]/dt = -k_1[B][P] + k_{-1}[BP]$$
$$d[P]/dt = -k_1[B][P] + k_{-1}[BP]$$
$$d[BP]/dt = k_1[B][P] - k_{-1}[BP]$$

Here, there are only two kinetic constants, k_1 and k_{-1}. k_1 can be independently estimated from the initial velocity (Figure S3).

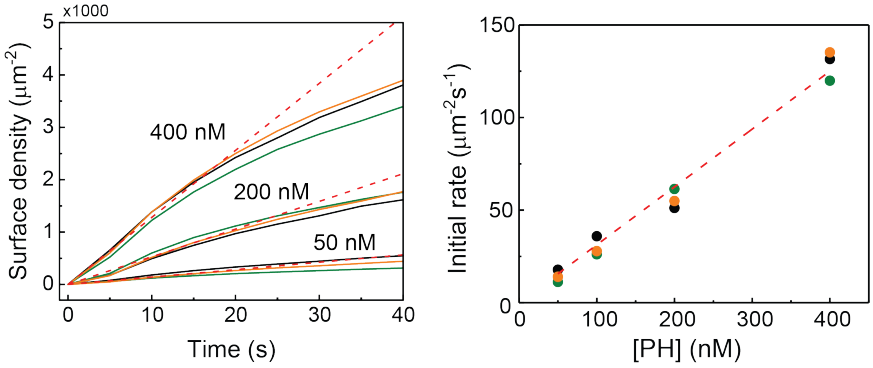

Figure S3. k_1 is the same for all constructs. The initial velocity was estimated by fitting the initial rate for each construct at 50 nM, 200 nM, and 400 nM solution protein concentration. The initial rates for all constructs agree, which is consistent with our assumptions about the sequential steps and independent binding (black = WT, orange = dimer mutant, green = peripheral site mutant).

The system involves both 2-dimensional (membrane-bound) and 3-dimensional (solution phase) species, which may complicate units. For simplicity, absolute number of molecules (in pmoles, 6.022×10^{-11}) instead of concentration was used to represent the amount of each species in the experimentally defined conditions. With this choice of units, the forward reaction rate constants are in $\text{pmoles}^{-1}\text{s}^{-1}$ and reverse rate constants are in s^{-1}. The surface density of membrane-bound species measured by FCS-calibrated TIRF was likewise converted to pmole. Fitting the peripheral site mutant adsorption data with k_1 fixed at the measured value, k_{-1} was estimated by least square optimization (Figure S4A).

For the dimer interface mutant, $k_3 = 0$ as it cannot dimerize. The rate equations are:

$$d[B]/dt = -k_1[B][P] + k_{-1}[BP]$$
$$d[P]/dt = -k_1[B][P] + k_{-1}[BP] - k_2[BP] + k_{-2}[BP_2]$$
$$d[BP]/dt = k_1[B][P] - k_{-1}[BP] - k_2[P][BP] + k_{-2}[BP_2]$$
$$d[BP_2]/dt = k_2[BP][P] - k_{-2}BP_2$$

Here, there are four kinetic constants, k_1, k_{-1}, k_2, and k_{-2}. k_1 and k_{-1} are fixed at the values obtained from the peripheral site mutant data in the previous step, so only k_2 and k_{-2} need to be estimated. In this case,

the sum $[BP] + [BP_2]$ was optimized to the dimer interface mutant adsorption data, since both species contribute to the TIRF intensity equally (Figure S4B).

For the last step, the same approach was used to estimate k_{3a}, k_{-3a} with Model A, and k_{3b}, k_{-3b} with Model B. Here, the membrane-bound species present in the system are BP, BP_2, and either of the dimeric species B_2P_3 or B_2P_4. Since the dimeric species are expected to contribute twice as much to the TIRF intensity, the sum $[BP] + [BP_2] + 2[B_2P_3]$ and $[BP] + [BP_2] + 2[B_2P_4]$, for Model A and B, respectively, were optimized to the wild type adsorption data (Figure S4C and S4D, respectively).

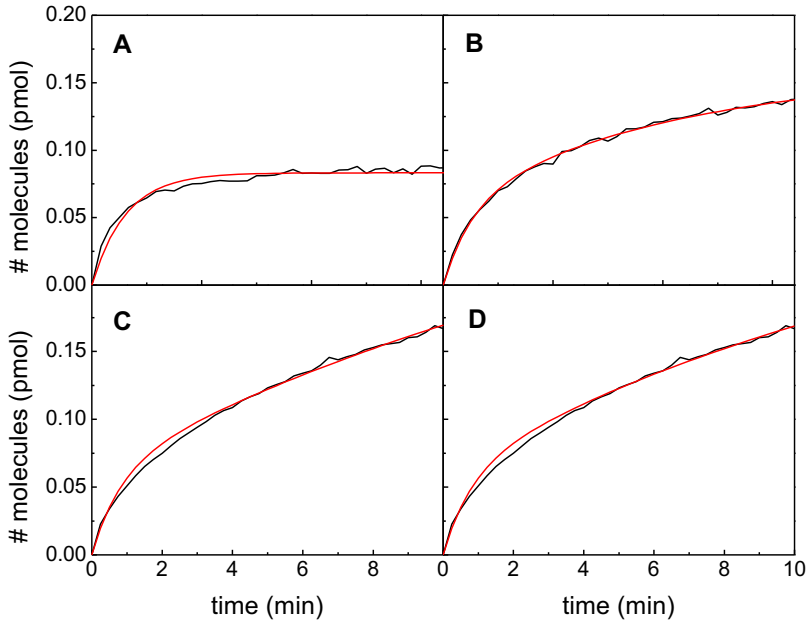

Figure S4. Fitting of rate constants to experimental TIRF adsorption data. Rate constants were fit for two of the models considered (Figure 4). Adsorption data for each mutant was fit sequentially, based on the observations from the FCS data. (A) After the initial rate was fit, the adsorption data from the peripheral site mutant was fit to find k_{-1}. (B) Adsorption data for the dimer interface mutant was fit to find k_2 and k_{-2}. (C) The WT adsorption data was fit to find k_{3a}, k_{-3a}, k_{3b}, k_{-3b}.

The following table summarizes the estimated kinetic constants:

Reaction	Forward rate constant ($pmoles^{-1}s^{-1}$)	Reverse rate constant (s^{-1})
$B + P \leftrightarrow BP$	$k_1 = 4.7 \times 10^{-4}$	$k_{-1} = 1.5 \times 10^{-3}$
$BP + P \leftrightarrow BP_2$	$k_2 = 7.8 \times 10^{-4}$	$k_{-2} = 3.1 \times 10^{-3}$
$2BP_2 \leftrightarrow B_2P_4$	$k_{3a} = 1.0$	$k_{-3a} = 5.0 \times 10^{-2}$
$BP_2 + BP \leftrightarrow B_2P_3$	$k_{3b} = 2.5 \times 10^{-2}$	$k_{-3b} = 1.5 \times 10^{-4}$

Table S1. Rate constants fit from experimental TIRF adsorption data. These are the rate constants fit as described in figure S4.

4. Calculating the activation probability for dimerization vs. tetramerization

This section will detail activation probability shown in Figure 6. For the dimerization case, the model is

(1) $\text{Btk} + \text{PIP}_3 \underset{k_{-1}}{\overset{k_1}{\rightleftharpoons}} \text{Btk:PIP}_3$

(2) $\text{Btk:PIP}_3 + \text{PIP}_3 \underset{k_{-2}}{\overset{k_2}{\rightleftharpoons}} \text{Btk:(PIP}_3)_2$

(3) $2\text{Btk:(PIP}_3)_2 \underset{k_{-3}}{\overset{k_3}{\rightleftharpoons}} \text{Btk}_2\text{:(PIP}_3)_4 \xrightarrow{k_{cat}} 2p\text{Btk:(PIP}_3)_2$

(4) $p\text{Btk:(PIP}_3)_2 \underset{k_2}{\overset{k_{-2}}{\rightleftharpoons}} p\text{Btk:PIP}_3 + \text{PIP}_3$

(5) $p\text{Btk:PIP}_3 \underset{k_1}{\overset{k_{-1}}{\rightleftharpoons}} p\text{Btk} + \text{PIP}_3$

And for the tetramerization case,

(1) $\text{Btk} + \text{PIP}_3 \underset{k_{-1}}{\overset{k_1}{\rightleftharpoons}} \text{Btk:PIP}_3$

(2) $4\text{Btk:PIP}_3 \underset{k_{-3}}{\overset{k_3}{\rightleftharpoons}} \text{(Btk:PIP}_3)_4 \xrightarrow{k_{cat}} 4p\text{Btk:PIP}_3$

(3) $p\text{Btk:PIP}_3 \underset{k_1}{\overset{k_{-1}}{\rightleftharpoons}} p\text{Btk} + \text{PIP}_3$

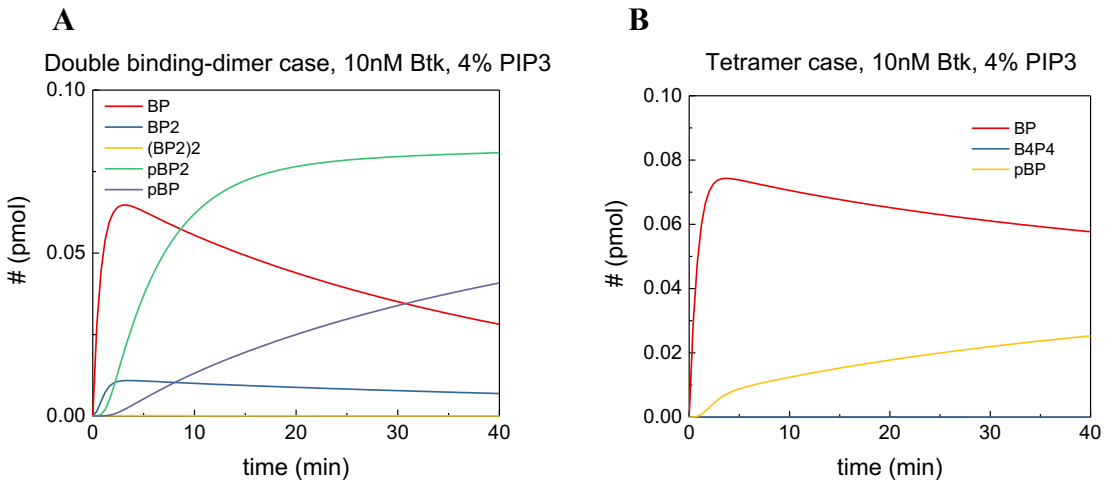

Figure S5. Simulated amount of each species for double binding or tetramer case. The time course for different species plotted for 40 minutes in either case. The kinetic rate constants calculated from Model A and k_{cat} from Src (1) were used. (A) Shows the double binding-dimer case and (B) shows the tetramer case.

The activation probability was defined as the number of membrane-bound phosphorylated Btk divided by all membrane-bound Btk at equilibrium. In other words, for the dimerization case,
$P_d = ([p\text{Btk:PIP}_3] + [p\text{Btk:(PIP}_3)_2])/ ([p\text{Btk:PIP}_3] + [p\text{Btk:(PIP}_3)_2] + [\text{Btk:PIP}_3] + [\text{Btk:(PIP}_3)_2])$

And for the tetramerization case,
$P_t = [p\text{Btk:PIP}_3]/ ([p\text{Btk:PIP}_3] + [\text{Btk:PIP}_3])$
Same calculations were performed for a range of PIP_3 surface densities to obtain Figure 6C.

5. Effects of other anionic lipids

Other PH domains are known to interact with negatively charged lipids with low specificity (2, 3). Previous solution-based studies have shown that the Btk PH domain is highly specific for PIP_3 over other types of anionic lipids (1, 4). Accordingly, no recruitment of the PH-TH module was observed for SLBs containing up to 10% PS or 4% PIP_2. These densities were used in order to match the charge or PIP lipid density, respectively, found in 4% PIP_3 SLBs. These observations suggest that the initial binding of the PH-TH module to the membrane is through specific PIP_3 binding to the canonical lipid binding site rather than due to nonspecific charge interactions. Furthermore, inclusion of negatively charged PS does not promote dimerization in 1% PIP_3 bilayers, indicating that dimerization occurs through specific interactions with PIP_3.

In the case of PS, the lipid shows no enhancement of dimerization in the 1% PIP_3 case. When combining PIP_2 with PIP_3, an intermediate level of dimerization can be achieved, however the presence of PIP_2 cannot recapitulate the dimer populations observed for 4% PIP_3, even at very high Btk PH-TH surface density. It should be noted that Btk PH-TH does not associate to bilayers containing only PIP_2, in the absence of PIP_3.

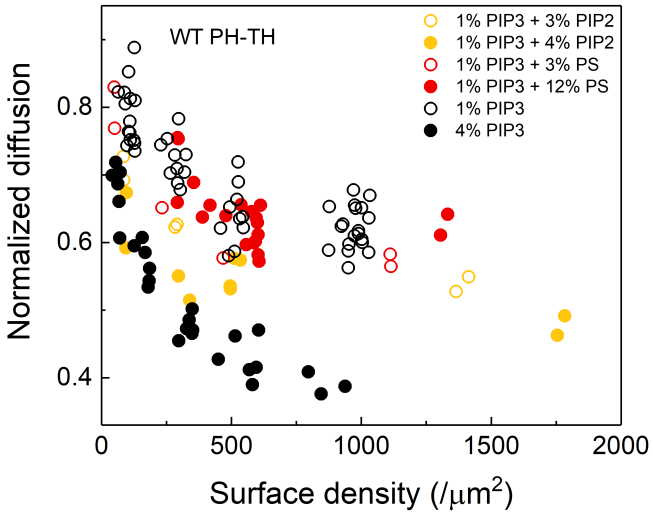

Figure S6. Effects of other anionic lipids. Btk PH-TH module dimerization for various lipid bilayer compositions, including PIP_3.

6. Effect of IP_6

As it was not previously known whether the peripheral site is specific for IP_6 alone, experiments were performed to confirm that IP_6 does not enhance dimerization of Btk PH-TH on PIP_3 containing bilayers. This is true for the peripheral site mutant as well. In fact, IP_6 seems to directly compete with PIP_3 and will compete Btk PH-TH off the membrane at high enough concentrations.

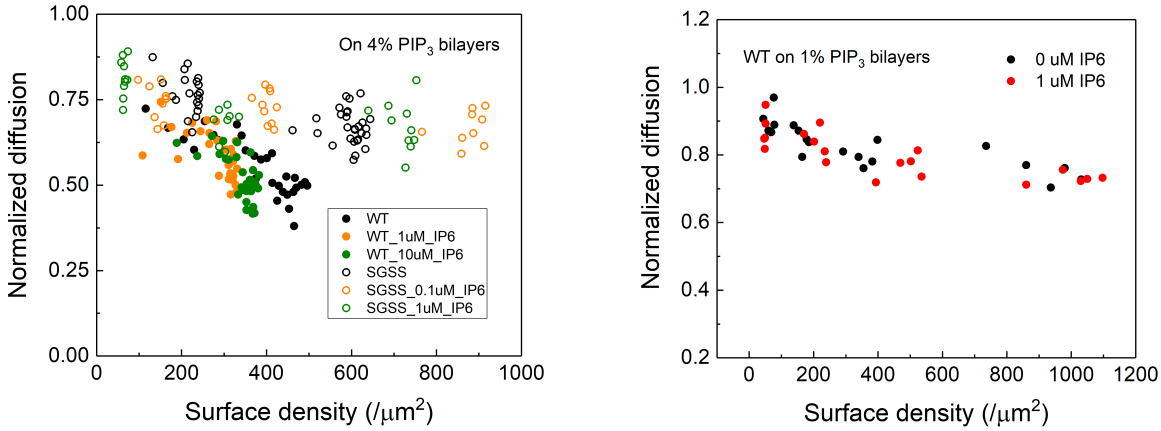

Figure S7. Effect of IP6 on PH-TH module dimerization. (*Left*) On 4% PIP_3 bilayers, the wild type PH-TH and the peripheral site mutant shows identical dimerization behavior with or without IP_6. (*Right*) On 1% PIP3 bilayers, the presence of IP_6 does not promote dimerization.

7. Expression level-dependent B-cell activation with Btk variants

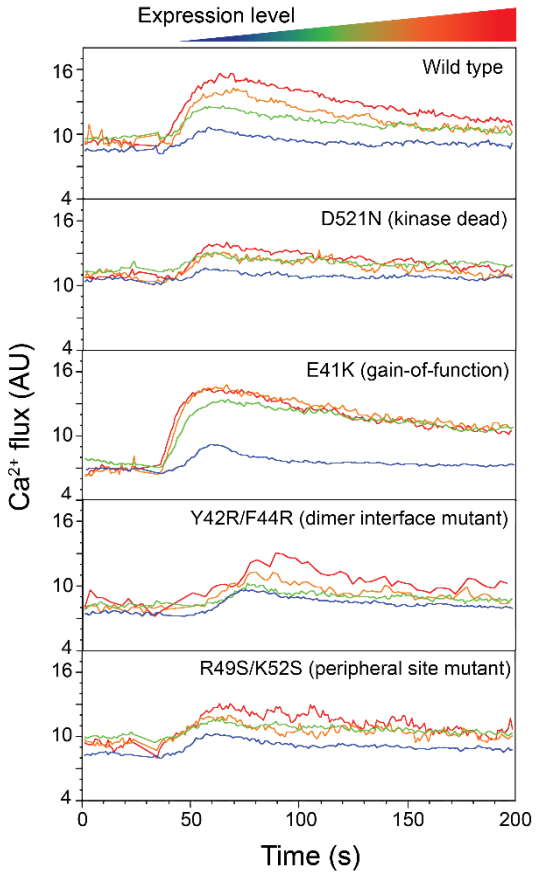

Figure S8. Expression level-dependent B-cell activation for Btk variants. The calcium flux upon activation by anti-BCR antibody are shown for wild type, D521N (kinase dead, negative control), E41K (gain-of-function, positive control), Y42R/F44R (dimer interface mutant), and R49S/K52S (peripheral site mutant). The dimer interface and peripheral site mutants show calcium flux comparable to that of D521N, demonstrating that both dimerization and the peripheral PIP_3 binding are important for Btk activation.

8. E41K PH-TH binding to supported lipid bilayers

Mutation of Glu 41, a residue near the canonical lipid binding site of the PH domain, confers specificity for PIP_3 over PIP_2 (5). The mechanism of E41K constitutive activity is still an open question, and in order to try to explore this mechanism we investigated the loss of specificity upon introducing the mutation to the PH-TH module alone. Based on these studies it seems that the E41K PH-TH module shows a similar binding affinity for PIP_2 and PIP_3, however the binding affinity compared to WT is much weaker in both cases.

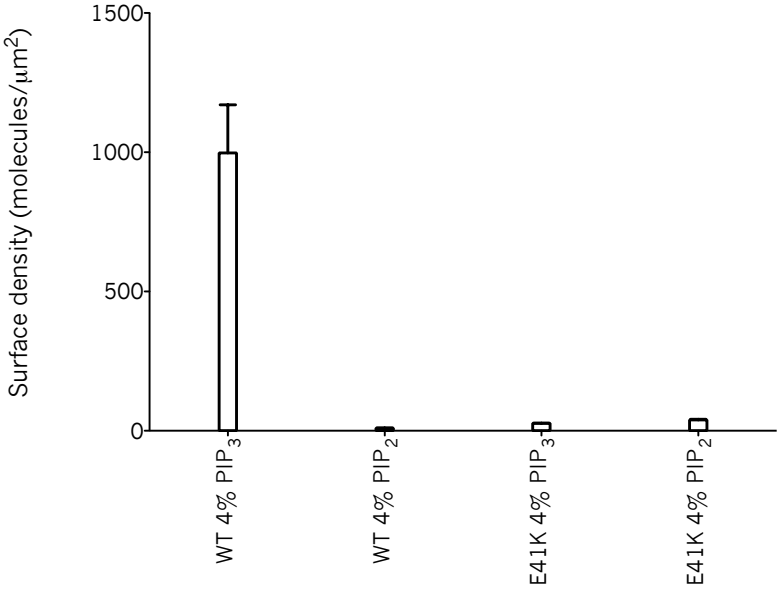

Figure S9. E41K mutation to the PH-TH module in vitro leads to loss of specificity and weaker binding affinity. Here we show the surface density of GFP labeled PH-TH measured by FCS for either WT or E41K on both 4% PIP_3 and 4% PIP_2 bilayers. The solution concentration of PH-TH in each case was kept constant at 20 nM, and measurements were made after 40 minutes of incubation with the supported lipid bilayers.

9. Method details

Protein purification

pET-28 plasmid containing residues 1-172 of bovine Btk fused to C-terminal eGFP or mCherry and N-terminal His6 was transformed into BL21(DE3) cells with GroES/GroEL and YopH. After growth and lysis, the proteins were purified by a Ni-NTA affinity chromatography, and the His tag was removed, followed by size exclusion chromatography.

Supported lipid bilayers (SLB)

SLBs were formed by rupturing small unilamellar vesicles, prepared by probe sonication, on glass substrates cleaned by piranha etch. Other bilayer components such as $PI(3,2,4)P_3$ (PIP_3), $PI(4,5)P_2$ (PIP_2), DOPS were also purchased from Avanti. A trace amount (0.005 mol %) of Texas Red DHPE (ThermoFisher Scientific) was also included. The bilayers were prepared in ibidi sticky-slide VI 0.4 microfluidic chambers (ibidi GmbH). The final buffer (pH 7.4) was composed of the following: 40 mM HEPES, 100 mM NaCl, 10 mM BME, 0.1 mg/mL casein.

Fluorescence correlation spectroscopy (FCS) and FRET

The light source was a pulsed (100 ps) supercontinuum laser (NKT Photonics). The average excitation power for a typical FCS measurement was 0.5 and 1 μW for 488 and 568 nm, respectively. The signals were collected by the objective and passed a 50-μm pinhole, then detected by avalanche photodiode detectors (Hamamatsu), and processed by a hardware correlator (Correlator.com). The focus radii, calibrated with bilayers containing known amounts of fluorescent lipids, were 0.20 ± 0.01 μm and 0.22 ± 0.01 μm for 488 and 568 nm, respectively. For TCSPC the measurements were performed on the same system, but the signals were processed by a TCSPC card (PicoQuant). The resulting photon arrival time histograms were fit to a single exponential decay with lifetime τ.

Adsorption kinetics

These experiments were carried out on a Nikon Ti-E, with objective-type TIRF illumination (NA 1.49). The excitation source was a 488 nm diode laser (Coherent Cube), and the camera was an Andor iXon-Ultra 897 EMCCD (Andor Technology). The analysis of kinetic time courses simulated by numerically solving coupled kinetic equations was done in MATLAB. (See SI Appendix Section 3 for details).

Btk knockout B-cell calcium activity assay

Btk-deficient DT40 cells were transiently transfected with 15 μg DNA of pEGFP-N1-nBtk (wild type or mutant) by electroporation (Biorad). The cells were then washed in cell loading media (CLM) containing 1 mM Ca^{2+}, 1 mM Mg^{2+}, 1% FBS and loaded with 1mg/mL indo-1 AM (Life Technologies) and 1mM probenecid for 30 minutes at 37°C. Then, they were washed twice with CLM, resuspended in 1 mL CLM, and rested for 15 minutes prior to analysis. Calcium flux was monitored by flow cytometry (BD LSRFortessa) before and after stimulation with 1:1000 dilution of anti-chicken BCR monoclonal antibody M4 or 1 μM Ionomycin.

References

1. Wang Q*, et al.* (2015) Autoinhibition of Bruton's tyrosine kinase (Btk) and activation by soluble inositol hexakisphosphate. *Elife* 4.
2. Lemmon MA (2008) Membrane recognition by phospholipid-binding domains. *Nat Rev Mol Cell Bio* 9(2):99-111.
3. Kavran JM*, et al.* (1998) Specificity and promiscuity in phosphoinositide binding by Pleckstrin homology domains. *J Biol Chem* 273(46):30497-30508.
4. Rameh LE*, et al.* (1997) A comparative analysis of the phosphoinositide binding specificity of pleckstrin homology domains. *J Biol Chem* 272(35):22059-22066.
5. Pilling C, Landgraf KE, & Falke JJ (2011) The GRP1 PH domain, like the AKT1 PH domain, possesses a sentry glutamate residue essential for specific targeting to plasma membrane PI(3,4,5)P(3). *Biochemistry-Us* 50(45):9845-9856.